International Journal of Nanomedicine

Dovepress
open access to scientific and medical research

Open Access Full Text Article

ORIGINAL RESEARCH

Macro-Microporous Surface with Sulfonic Acid Groups and Micro-Nano Structures of PEEK/Nano Magnesium Silicate Composite Exhibiting Antibacterial Activity and Inducing Cell Responses

This article was published in the following Dove Press journal:
International Journal of Nanomedicine

Yunfei Niu[1]
Lieping Guo[2]
Fangyong Hu[3]
Lishu Ren[4]
Qirong Zhou[1]
Jiangying Ru[3]
Jie Wei[4]

[1]Department of Orthopaedics, Changhai Hospital, Second Military Medical University, Shanghai 200433, People's Republic of China; [2]Department of Oncology, Shanghai Eastern Hepatobiliary Surgery Hospital, Shanghai 200438, People's Republic of China; [3]Department of Orthopaedics, The Affiliated Hospital of Yangzhou University, Yangzhou University, Yangzhou 225009, People's Republic of China; [4]Key Laboratory for Ultrafine Materials of Ministry of Education, East China University of Science and Technology, Shanghai 200237, People's Republic of China

Purpose: To improve the surface bio-properties of polyetheretherketone (PEEK)/nano magnesium silicate (n-MS) composite (PC).

Materials and Methods: The surface of PC was firstly treated by particle impact (PCP) and subsequently modified by concentrated sulfuric acid (PCPS).

Results: PCPS surface exhibited not only macropores with sizes of about 150 μm (fabricated by particle impact) but also micropores with sizes of about 2 μm (created by sulfonation of PEEK) on the macroporous walls, and sulfonic acid (-SO_3H) groups were introduced on PCPS surface. In addition, many n-MS nanoparticles were exposed on the microporous walls, which formed micro-nano structures. Moreover, the surface roughness and hydrophilicity of PCPS were obviously enhanced as compared with PC and PCP. Moreover, the apatite mineralization of PCPS in simulated body fluid (SBF) was obviously improved as compared with PC. Furthermore, compared with PC and PCP, PCPS exhibited antibacterial performances due to the presence of -SO_3H groups. In addition, the responses (eg, adhesion and proliferation as well as differentiation) of bone marrow mesenchymal stem cell of rat to PCPS were significantly promoted as compared with PC and PCP.

Conclusion: PCPS with macro-microporous surface containing -SO_3H groups and micro-nano structures exhibited antibacterial activity and induced cell responses, which might possess large potential for bone substitute and repair.

Keywords: PEEK based composite, sulfonation, macro-microporous surface, antibacterial performances, cell responses

Introduction

As for bearing bone substitute and repair, implantable biomaterials should possess not only high mechanical properties but also excellent biocompatibility and osteogenic activity, which promotes bone regeneration and osseointegration that ensures early load/fixation and long-term stability of the implants in vivo.[1,2] Bacterial infection is the main cause of the failure of implants in orthopedics, thus implantable biomaterials with antibacterial performances can inhibit bacterial infection and thereby maintain long-term stability of the implants.[3] As a result, implantable biomaterials with osteogenic activity and antibacterial performances are two key factors to determine the success of the bone implantation.[4] As one of implantable biomaterials, polyetheretherketone (PEEK) has been widely applied as implants in

Correspondence: Yunfei Niu
Department of Orthopaedics, Changhai Hospital, Second Military Medical University, Shanghai 200433, People's Republic of China
Email nyunfei1219@163.com

Jiangying Ru
Department of Orthopaedics, The Affiliated Hospital of Yangzhou University, Yangzhou University, Yangzhou 225009, People's Republic of China
Tel +86-21-311 61690
Fax +86-21-31161016
Email rujiangying@163.com

submit your manuscript | www.dovepress.com
DovePress
http://doi.org/10.2147/IJN.S238287

clinic for many years because of biocompatibility and mechanical properties as well as elastic modulus similar to the bone of human, etc.[5,6] However, PEEK is a biologically inert material, which does not have the capability to promoting cells attachment and proliferation as well as differentiation, thereby displays poor osteogenic activity.[6] Therefore, enhancements of the bio-performances of PEEK, especial osteogenic activity and achievement of osseointegration, are still challenges in orthopedic applications.

To improve the osteogenic activity of PEEK, many ways of surface treatments have been researched and developed (eg physical, chemical or biological ways) to modify PEEK surface, which aimed to accelerate bone regeneration and osseointegration.[7–9] However, the osteogenic activity of PEEK was not significantly enhanced by these treatments (eg, plasma treatment, grafting functional group and biomolecules, etc.) due to their unstable properties on PEEK.[7–9] In addition, for surface modifications, the general ways were coatings of bioactive materials (eg hydroxyapatite, bioglass) on PEKK surface, which have been confirmed to be effective in the acceleration of bone regeneration and osseointegration.[10,11] However, because of the weak bonding strength between the coatings and substrates, the coatings might be detached from PEEK surface, which dramatically reduced the osteogenic activity.[10–13] Furthermore, the detached coating debris might cause bone resorption, leading to the failure of implantation.[10–13]

Over the past decades, inorganic/organic biocomposites were developed by incorporation of inorganic bioactive materials (such as bioglass/ceramic) into organic polymers (such as polylactic acid, polyamide and polyethylene) for bone repair, which significantly enhanced the osteogenic activity of the biocomposites.[14,15] Previous studies have reported that PEEK-based composites were fabricated by incorporating of the bioactive materials into PEEK, which improved mechanical properties and bioactivity of the composites compared with PEEK.[16,17] Although the composites containing bioactive materials exhibited improved mechanical properties and bioactivity, most of the bioactive materials were dispersed into PEEK matrix, which did not significantly improve the surface bioactivity (only a few bioactive materials exposing on the surface).[16,17] As non-degradable biomaterials for permanent implantation, surface properties (eg chemical composition and topography) have critical effects on the bio-performances.[17] Therefore, it is necessary to modify the surface of PEEK-based composites to further improve the surface osteogenic activity.

Nano magnesium silicate (n-MS) based glass with large specific surface area displayed higher bioactivity with rapid apatite formation on the surface in simulated body fluid (SBF).[18] In previous studies, PEEK-based composite (PC) has been developed, and the bioactivity of the composite was improved as compared with PEEK.[19] To further improve the surface bio-properties of PC, in this study, the surface of PC was firstly treated by particle impact to fabricate macropores on PC surface (PCP), which was subsequently modified by concentrated sulfuric acid (H_2SO_4) to produce micropores on the macroporous walls of PCP (PCPS). The purpose of the study was to create macro-microporous surface containing functional groups of sulfonic acid (-SO_3H) and micro-nano structures on PCPS, which could exhibit antibacterial performances and induce cells responses. To confirm the hypotheses, the surface characteristics (morphology, roughness, hydrophilicity, functional groups and apatite mineralization) and antibacterial performances as well as rat bone mesenchymal stem cells (BMSC) responses (eg, adhesion, proliferation and differentiation) to PCPS were investigated as compared with PCP and PC.

Materials and Methods

Preparation and Characterization of Samples

Nano magnesium silicate (n-MS) powders were prepared according to the previous study.[18] Polyetheretherketone (PEEK, Victrex, UK) and n-MS powders were mixed and ground in a star-shaped ball mill for 4 hours to obtain a uniform mixed powder, which contained n-MS of 40 wt %. The mixed powders containing PEEK and n-MS were added into ethanol solution (200 mL) with ultrasonic stirring (2 hours). The dispersion was centrifuged, and the mixture was obtained, which was dried at 55°C in a draught drying cabinet (DHG-9070A, Bluepard, Shanghai, China). The dried mixed powders containing PEEK and n-MS were placed into the stainless-steel mold. Disc-shaped samples with dimensions of Φ12 × 2 mm were compressed by a pressing machine (YP-15T, Jinfulun Technology Co., Ltd, China) with a pressure of 4 MPa for 2 min, which were sintered in the muffle furnace (at 350°C) for 4 hours.

The obtained samples (PC) were mechanically polished and ultrasonically cleaned in acetone and ethanol as well

as distilled water. The samples were dried at room temperature and then surface of the samples was impacted by aluminum oxide (Al_2O_3) particles with the size of around 250 μm with a Suction Blast Cabinet (JG-5832, China). Samples treated by particle impact (PCP) were further sulfated with concentrated sulfuric acid (98%) with magnetic stirring for 10 min at room temperature. After the sulfonation reaction was completed, the samples (PCPS) were taken out from the sulfuric acid solution and immersed in distilled water for 15 minutes to remove surface residues, and then the samples were hydrothermally treated at 120°C for 4 hours.

The surface morphology and composition of the samples (PC, PCP and PCPS) were characterized by scanning electron microscopy (SEM, Hitachi, Japan), energy dispersive spectrometry (EDS, Hitachi, Japan), X-ray photoelectron spectroscopy (XPS, Thermo Fisher, USA). The structure and composition of the samples were characterized by Fourier transform infrared spectrometry (FT-IR, Nicolet, USA) and X-ray diffraction (XRD, Kyoto, Japan). The surface morphology as well as surface roughness (Ra) of the samples was detected by laser confocal 3D microscope (VK-X110, Keyence Co., Japan).

Apatite Mineralization in SBF

Apatite mineralization of samples was determined by observing the surface morphology and compositions after the samples were immersed into simulated body fluid (SBF) for different time. The SBF solution was prepared as reported in a previous study.[19,20] The samples (PC, PCP and PCPS) were immersed into SBF solution (solid/liquid ratio:1cm^2/20 mL), which were placed into a constant temperature shaking box (HZQ-X300, yiheng science instruments Co., Ltd., China) at 37°C for 7 days. The samples were removed out and cleaned in deionized water for 2 times, and then dried in vacuum (at 50°C) for 24 hours. The surface morphology and composition of the dried samples were determined using SEM and EDS, respectively.

Antibacterial Activity

The antimicrobial properties of the samples were evaluated using the method of bacterial counting. Antibacterial experiments were performed using *Escherichia coli* (*E. coli*, ATCC 25922) and *Staphylococcus aureus* (*S. aureus*, ATCC 25923). The samples (PC, PCP and PCPS) with the size of Φ12 × 2 mm were sterilized using a high-temperature sterilizer before the experiments. The broth medium was used to culture bacteria of both *E. coli* and *S. aureus*, which were seeded on the samples. The samples were then placed into a 24-well plate, and 1 mL of bacterial stock solution (1×10^6 CFU/mL) was added into each well. The bacteria were co-cultivated with samples (bacterial suspension) at 37°C for 24 h in humid conditions, and then put into the sterilized centrifugal tube containing 5 mL of sterile phosphate buffer saline (PBS). The centrifugal tube was agitated vigorously (centrifugation) for 30s using a vortex mixer to dissociate bacteria from the samples. Afterwards, the dissociated bacteria suspensions were collected and diluted 10, 100, and 1000 times with sterilized PBS. The 100 μL of the diluted bacteria suspensions (*E. coli* and *S. aureus*) were separately aspirated, which were uniformly coated on the surface of the nutritional agar plate using a sterile glass coating bar. Subsequently, the agar plates were inverted and placed in a constant temperature incubator at 37°C for 24 hours. Finally, the number of bacterial colonies on the agar plate was calculated according to the national standard GB/T 4789.2. $Antibacterial\ ratio\ (\%) = \frac{Rc-Rt}{Rc} \times 100\%$, where *Rc* represents the number of the bacteria colonies on the PC surface, and *Rt* represents the number of bacterial colonies on the PCP and PCPS surfaces.

Cell Culture

The bone marrow mesenchymal stem cells (BMSC) of rat were purchased from the cell bank (Fudan University, Shanghai, China), which were cultured in α-MEM medium (Thermo Fisher Scientific Inc., USA). The medium contained 10 vol% fetal bovine serum (FBS, Gibco, USA) and 100 U/mL penicillin as well as 100 μg/mL streptomycin. The cells were placed in a CO_2 incubator with a humidity of 100%, CO_2 content of 5%, and temperature of 37°C. The medium was changed every 3 days.

Cell Adhesion

The samples (PC, PCP and PCPS) with the size of Φ12 × 2 mm were sterilized in a high-temperature sterilizing pot, and then placed in a 24-well plate. Trypsin (0.25%) was added into the culture dish to digest the cells (1 min), and then the medium was added into terminate the digestion, which was centrifuged to remove the upper medium. The cell culture medium was added again and the cells were counted. The cells were seeded on the samples (cell density: 2×10^4 cells/well), and the plates were placed into a cell culture incubator for 6, 12 and 24 hours, respectively. The cells on the samples were collected and the number of cells was counted using the CyQUANT® test

kit (Life technologies, Carlsbad, US). The cells were cultured in culture plate without sample as a control group. The number of cells was measured using a SpectraMax Microplate Detection System (Synergy HT, USA). Cell adhesion ratio was calculated according to the following formula: Cell adhesion ratio (%) = (number of cells on the samples/number of cells on the control) ×100. Culture plate without sample was used as a control (100% adhesion). The samples and the cells were co-cultured for 12 and 24 hours, and the adhesion and spreading of the cells on the samples were determined by applying confocal laser scanning microscopy (CLSM, Nikon, Japan). The cytoskeleton of cells on the samples was stained with 5 μg/mL phalloidin (FITC-Phalloidin; Sigma) for 40 min, and the nuclei were stained for 5 min by adding 4′,6′-diamidino-2-phenylindole (DAPI, Sigma) to the well of plates.

Cell Proliferation and Cell Morphology

Proliferation of BMSC on the samples (PC, PCP and PCPS) was analyzed using the CCK-8 kit. Firstly, the cells were co-cultured with the samples. At 1, 3 and 7 days after culturing, the cell culture medium was taken out, and 500 μL cell culture medium containing CCK-8 (50 μL) was added into each well (4 hours). Then, 100 μL liquid was taken out and added into the 96-well plate. Finally, the optical density (OD) of the culture solution was measured using a microplate reader (Synergy HT, USA) at a wavelength of 490 nm. The cells were co-cultured with the samples for 3 and 7 days. At the specific time point, the medium in the plate was removed, and the samples were washed by using PBS for 3 times. The cells were immobilized with 0.25% glutaraldehyde for 4 hours, and then the samples were subjected to gradient dehydration (concentration: 10%, 30%, 50%, 70%, 85%, 90%, 100%) with different concentrations of ethanol solution. The cell morphology on the samples was observed by SEM.

Alkaline Phosphatase Activity

Osteogenic differentiation of the cells on the samples was evaluated by detecting the alkaline phosphatase (ALP) activity at different time after culturing. The ALP activity was quantified by using ALP Kit (Nanjing Jiancheng Bioengineering Institute, China). The cells were co-cultured with samples for 7, 10, 14 days. At the specific time point, the medium was aspirated, and the samples were rinsed once with PBS. After that, 200 μL of Nonidet P-40 (NP-40, 1%) cell lysate was added into plates and incubated in a constant temperature incubator (37°C) for 90 min. On the basis of 50 μL of lysate, 100 μL of ALP working solution (containing 0.1 mol/L glycine and 1 mmol/L magnesium chloride hexahydrate, pH=9) was added into each well and incubated for 20 min. Subsequently, the above reaction was stopped by adding 100 μL of sodium hydroxide (NaOH) solution (0.1 mol/L). The absorbance was determined by using a microplate reader (at a wavelength of 405 nm). Then, 2 μL of liquid was taken from each well and 10 μL PBS was added, followed by the addition of 200 μL/well Bicinchoninic Acid assay reagent kit (Pierce Biotechnology Inc., USA). The total protein content (μg/mL) in the lysate was determined using bovine serum albumin as standard protein at a wavelength of 562 nm. The ALP activity was expressed as absorbance value at 405 nm/total protein content.

Statistical Analysis

All the experiments were performed at least 3 times, and the data were expressed as the mean ± standard deviation (M ± SD) with n=3. Statistical comparisons were carried out by one-way ANOVA with Tukey's post hoc test. The result was statistically significant ($p < 0.05$) by the standards of the study.

Results

Characterization of PC, PCP and PCPS

Both PC and PCP contained PEEK and n-MS, XRD patterns of PC, PCP and PCPS are shown in Figure 1A. For PC and PCP, the peaks at 2θ=18.91°, 20.80°, 23.16° and 28.68° corresponded to (110), (111), (200) and (202) crystal planes of PEEK, respectively.[21]

FTIR spectra of PC, PCP and PCPS are shown in Figure 1B. The peaks of PEEK at 1648 cm^{-1} corresponded to the vibration peak of C=O, the peaks at 1588 cm^{-1} and 1486 cm^{-1} corresponded to the in-plane stretching vibration of R-O-R in the benzene ring, the peak at 1226 cm^{-1} corresponded to the non-stretching vibration of R-O-R and the peaks at 1380cm^{-1} and 925 cm^{-1} corresponded to the R-CO-R benzene ring vibration.[21] The absorption peaks at 1093 cm^{-1} and 799 cm^{-1} were the antisymmetric stretching vibration peak of Si-O-Si, which were ascribed to the characteristic peaks of n-MS.[22] Moreover, the peak at 1255 cm^{-1} was related to O=S=O dissymmetric stretching, and the peak at 1050 cm^{-1} corresponded to S=O symmetric stretching.[23] The results indicated that sulfonic acid (-SO_3H) groups were introduced onto the PCPS surface by the sulfonation (PEEK

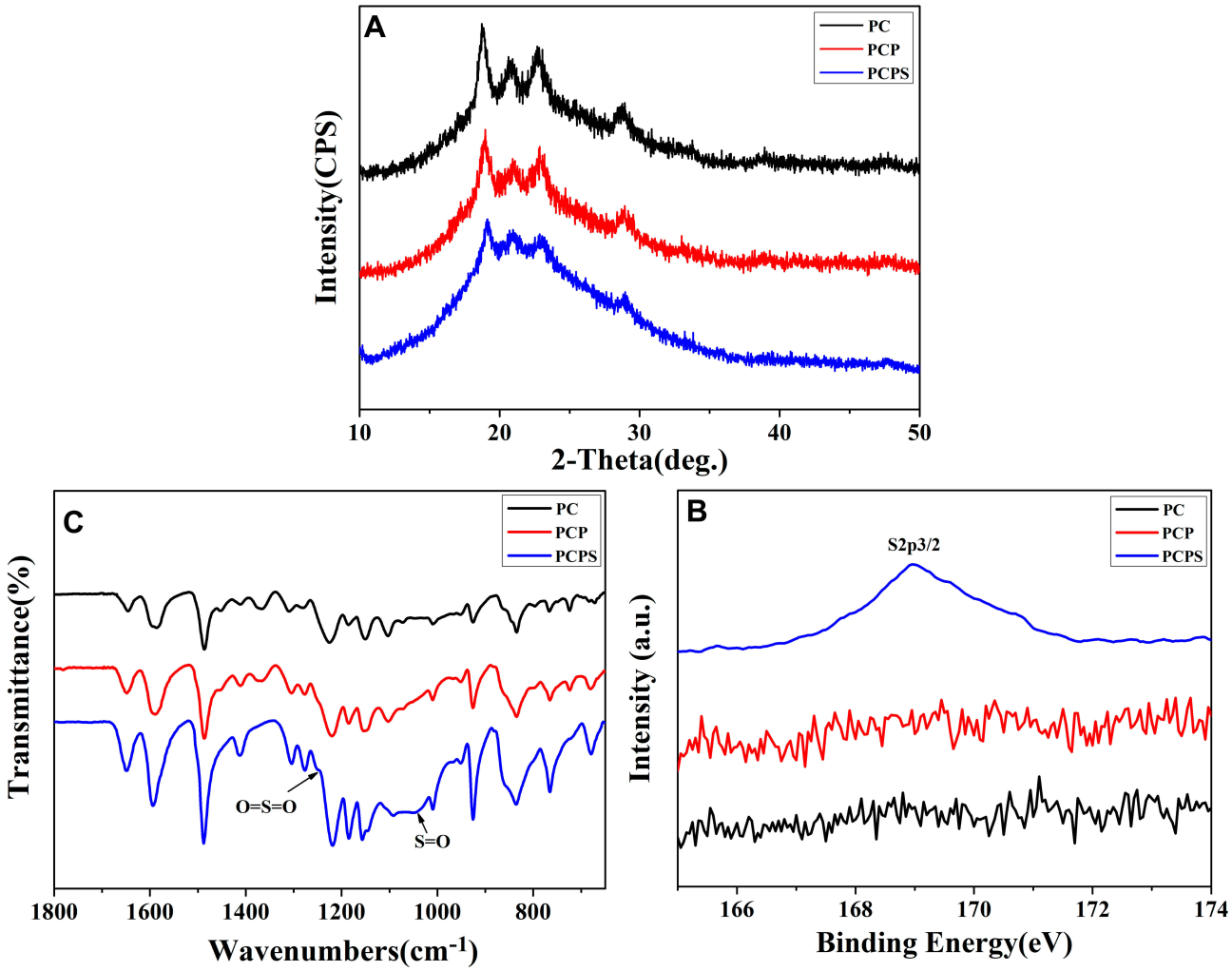

Figure 1 XRD (**A**), FTIR (**B**) and XPS (**C**) of PC, PCP and PCPS.
Abbreviations: XRD, X-ray diffraction; FTIR, Fourier transform infrared spectrometry; XPS, X-ray photoelectron spectroscopy; PC, polyetheretherketone/nano magnesium silicate composite; PCP, PC treated by particle impact; PCPS, PCP treated by concentrated sulfuric acid.

reaction with H_2SO_4). Figure 1C is the XPS spectra of PC, PCP and PCPS. The results revealed that the peak at 168.5 for PCPS corresponded to 2p3/2 of sulfur with a high oxidation state, which was the -SO_3H group.[24]

The SEM photographs of PC, PCP and PCPS are shown in Figure 2A–F. PC showed smooth surface (Figure 2A and B) while PCP exhibited rough surface with some exposed n-MCS particles (Figure 2C and D). After sulfonation treatment, many micropores were created on PCPS surface (Figure 2E–H). As shown in Figure 2G, the size of the micropores was about 2 μm and some n-MCS particles were dispersed on the microporous walls. As shown in Figure 2H, the n-MS particles with the size of about 100 nm were adhered onto the microporous walls.

Figure 3A and B shows the EDS spectra of PCP and PCPS. The elements of Mg and Si were found on PCP while the elements of Mg, Si and S were seen on PCPS. Figure 3C–E) reveals the EDS mapping of PCPS. The elements of Mg (c), Si (d) and S (e) were dispersed on PCPS. The sulfur content on PCPS was 1.21 ± 0.07 wt% after hydrothermal treatment at 120°C for 4 hours.

Laser microscope 3D photographs of surface morphology of PC, PCP and PCPS are shown in Figure 4. PC exhibited flat and smooth surface while PCP and PCPS showed some peaks and rough surface. As shown in Figure 4B and C, the surface of PCPS was obviously rougher than PCP. The surface roughness of samples is displayed in Figure 4D. Compared with PC (Ra=3.71 μm), the surface roughness of PCP (Ra=7.13 μm) obviously

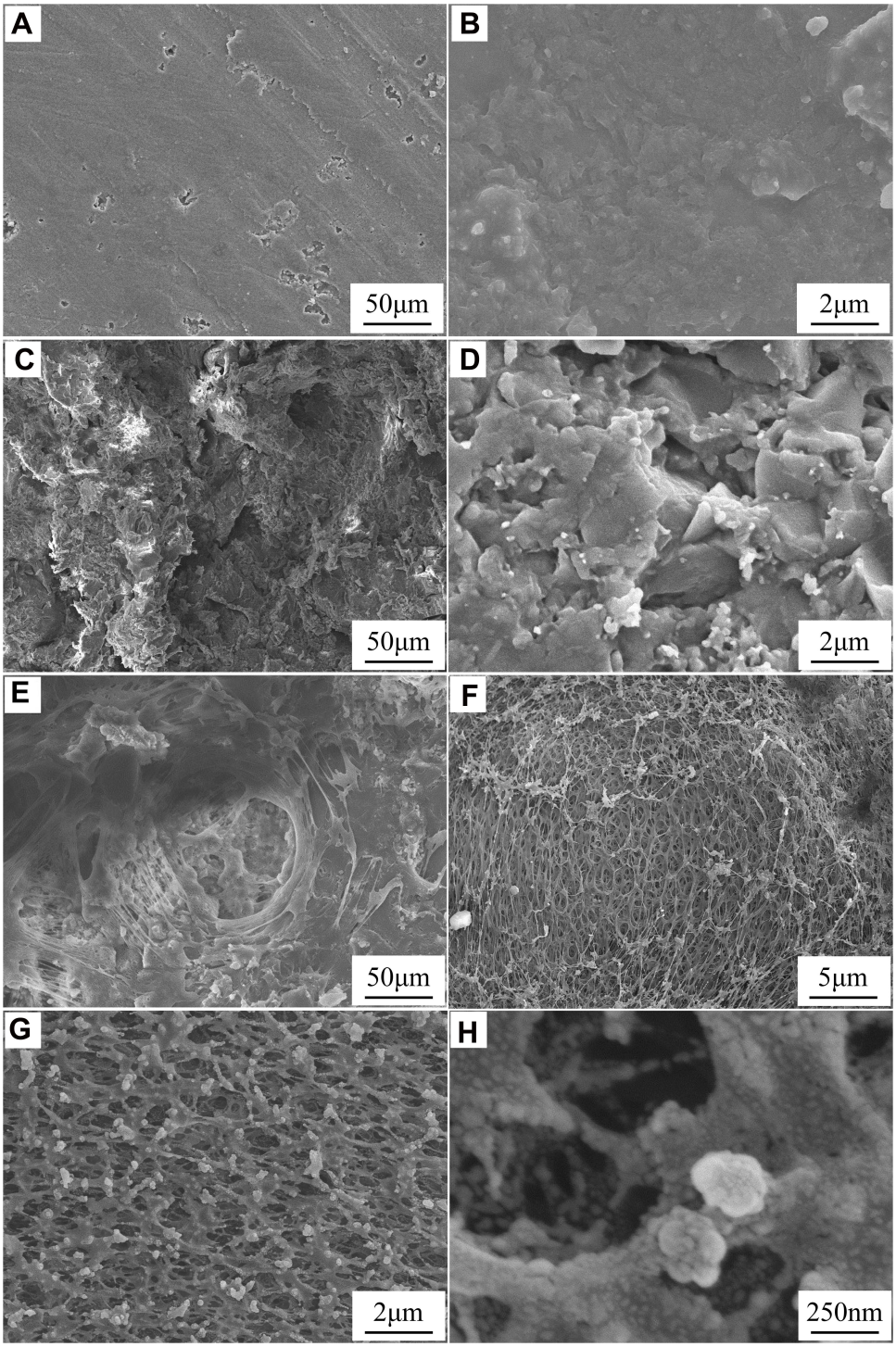

Figure 2 SEM photographs of surface morphology of PC (**A, B**), PCP (**C, D**) and PCPS (**E**–**H**) under different magnifications.
Abbreviations: SEM, scanning electron microscope; PC, polyetheretherketone/nano magnesium silicate composite; PCP, PC treated by particle impact; PCPS, PCP treated by concentrated sulfuric acid.

increased ($p<0.05$). Moreover, compared with PCP, the surface roughness of PCPS (Ra=10.84 μm) markedly increased ($p<0.05$). The surface water contact angle (CA_w) is displayed in Figure 4E. Compared with PC (CA_w=80°), the water contact angles of PCP (CA_w=72°) decreased ($p<0.05$). Moreover, compared with PCP, the water contact angles of PCPS (CA_w=56°) further decreased.

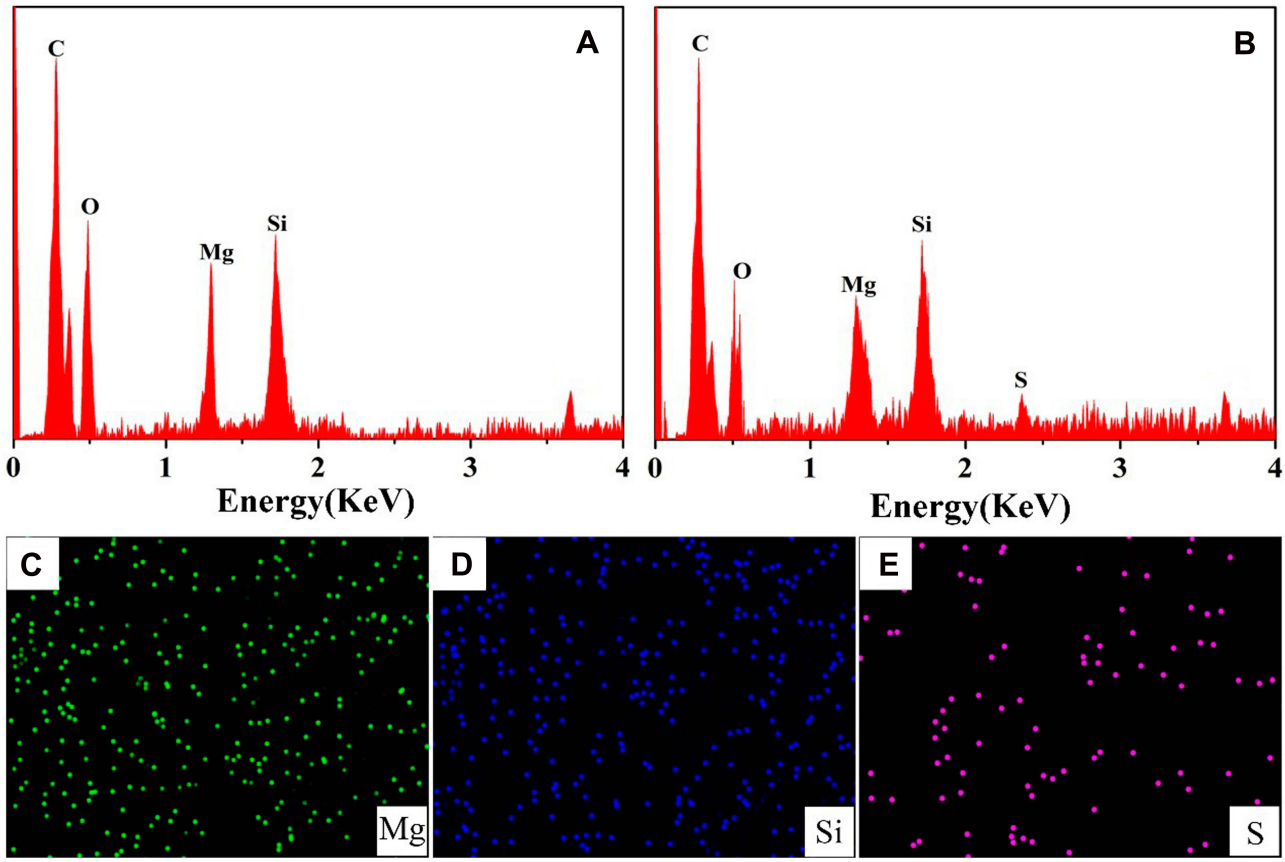

Figure 3 EDS spectra of PCP (**A**) and PCPS (**B**), and EDS mapping of Mg (**C**), Si (**D**) and S (**E**) elements distribution on PCPS surface.
Abbreviations: EDS, energy dispersive spectrometer; PC, polyetheretherketone/nano magnesium silicate composite; PCP, PC treated by particle impact; PCPS, PCP treated by concentrated sulfuric acid; Mg, magnesium; Si, silicon; S, sulfur.

Apatite Mineralization in SBF

Figure 5A–C shows the SEM photographs of surface morphology of PC (a), PCP (b) and PCPS (c) soaked into SBF for 7 days. The deposits were found on the surfaces of PC, PCP and PCPS. Compare to PC with the deposits containing some spherical particles, more spherical particles of deposits with dense structures were seen on both PCP and PCPS. Figure 5D–F shows EDS spectra of the deposits on samples soaked into SBF for 7 days. The deposits on all samples contained Ca and P elements. In addition, atom ratio of Ca to P (Ca/P ratio) was 1.61 ± 0.04, which was close to hydroxyapatite, indicating that the deposits were apatite.

Antibacterial Activity

Figure 6A shows the antibacterial properties of the samples after the *E. coli* and *S. aureus* cultured on the samples for 24 hours. A large number of colonies appeared in both PC and PCP, indicating no antibacterial activity. However, no bacterial colonies were observed in PCPS, indicating good antibacterial activity. Figure 6B shows the *E. coli* reduction rate for the samples. The percentage reduction of *E. coli* for PC and PCP was 0 while percentage reduction for PCPS was 98.29%. Figure 6C shows the percentage reduction of *S. aureus* for the samples. The percentage reduction of *S. aureus* for PC and PCP was 0 while percentage reduction for PCPS was 99.76%. The result indicated that PCPS exhibited antibacterial activity against *E. coli* and *S. aureus* while no antibacterial activity of both PC and PCP.

Cell Culture

Cell Morphology

Figure 7 shows the CLSM photographs of morphology of BMSC on PC, PCP and PCPS for different time. At 12 hours after culturing, the cells on PCPS and PCP spread better than PC. At 24 hours after culturing, more cells were observed on PCPS than PCP and PC. The results

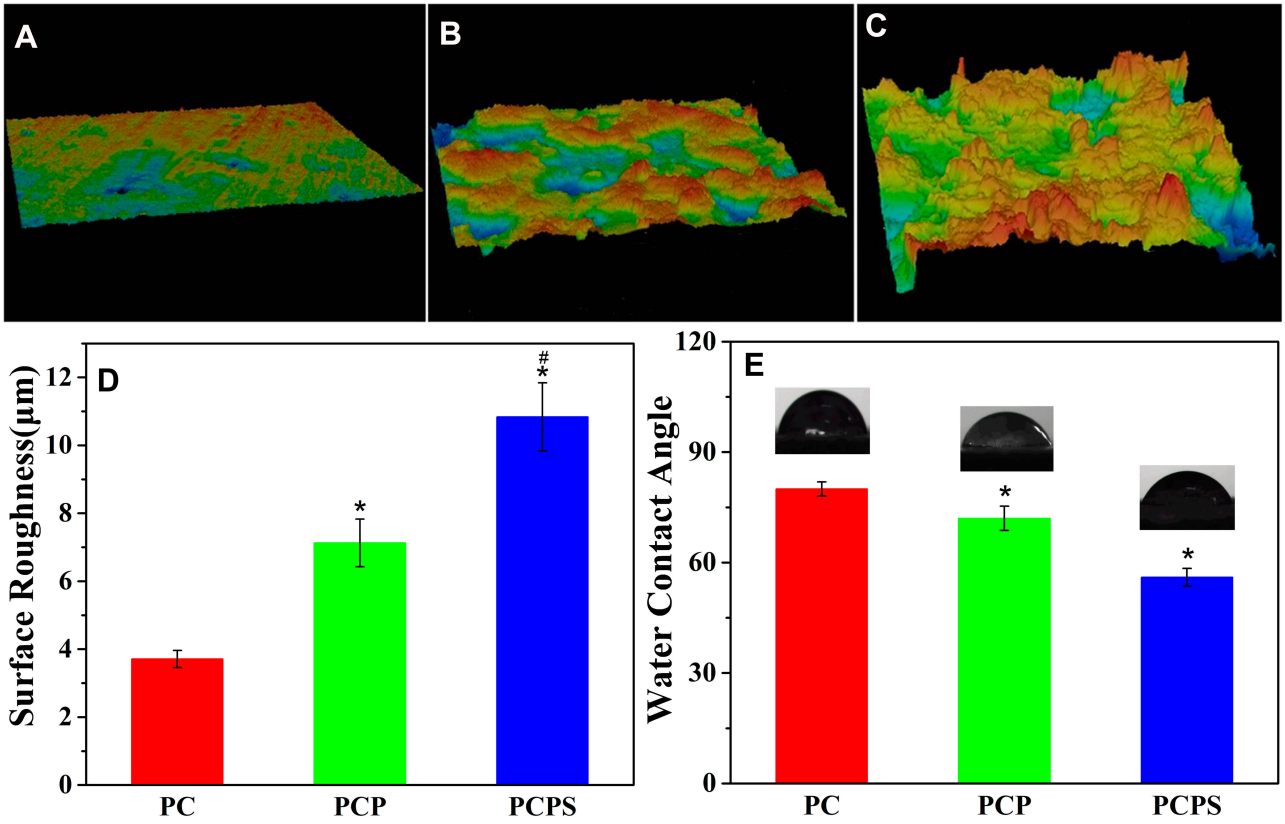

Figure 4 Laser microscope 3D photographs of surface morphology of PC (**A**), PCP (**B**) and PCPS (**C**), and surface roughness (**D**) and water contact angles (**E**) of PC, PCP and PCPS (*represents $p<0.05$, PCPS vs PC, PCP vs PC; #represents $p<0.05$, PCPS vs PCP).
Abbreviations: PC, polyetheretherketone/nano magnesium silicate composite; PCP, PC treated by particle impact; PCPS, PCP treated by concentrated sulfuric acid.

revealed that PCPS promoted the adhesion of the cells better than PCP and PC.

Figure 8 shows the SEM photographs of morphology of BMSC on PC, PCP and PCPS after culturing for different time. The cells were found to spread on all samples at both 3 and 7 days. At the same time point, some cells with less pseudopod spread on PC surface. However, many cells on both PCP and PCPS surfaces exhibited spreading morphology with more filopodia extending and anchoring on the microporous walls of the samples. The results indicated that more cells spread better on PCPS than PC and PCP.

Cell Adhesion, Proliferation and ALP Activity

Figure 9A shows the attachment ratios of cells on the samples at different time. The attachment ratios of cells on the samples increased with time. At 6 hours, no obvious difference for all samples was found. At 12 hours, the attachment ratios of cells on PCPS were remarkably higher than PCP and PC. At 24 hours, the attachment ratios of cells on PCPS were significantly higher than PCP, and PCP were higher than PC.

Optical density (indicating cell proliferation) of BMSC cultured on PC, PCP and PCPS for different time is displayed in Figure 9B. At 1 day, no obvious differences for all samples were found. At 3 days, the optical density of cells on PCPS was obviously higher than PCP and PC. At 7 days, the optical density of cells on PCPS was obviously higher than PCP, and PCP was higher than PC.

ALP activity (indicating cell differentiation) of BMSC on the samples for different time is displayed in Figure 9C. The ALP activity of the cells on all samples significantly enhanced with time. In addition, at 7, 10 and 14 days after culturing, the ALP activity of cells on PCPS was obviously higher than PCP, and PCP was higher than PC.

Discussions

For successful bone substitute and repair, it is expected that the implantable biomaterials have osteogenic activity as well as antibacterial properties, which can achieve integration with host bone that lead to the initial fixation and long-term stability as well as resistance infection.[1,3] Surface characteristics (such as morphology and texture,

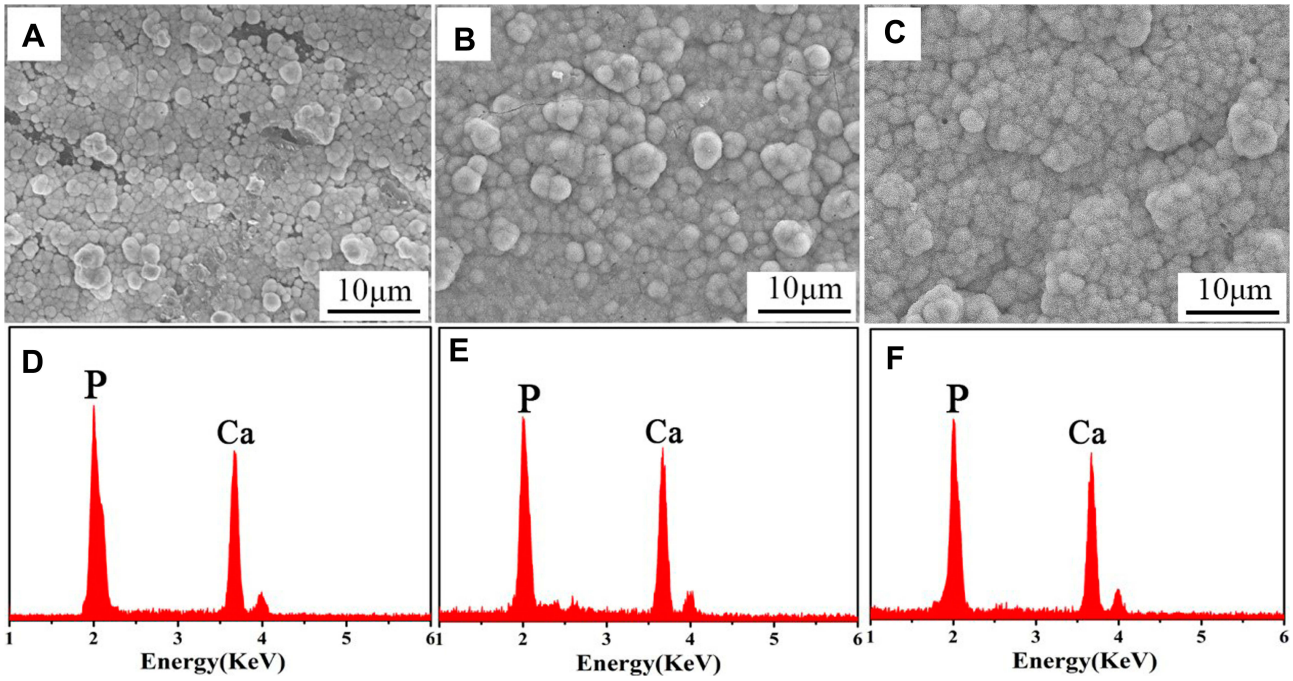

Figure 5 SEM photographs of surface morphology of PC (**A**), PCP (**B**) and PCPS (**C**) soaked into SBF for 7 days, and EDS spectra of deposits on PC (**D**), PCP (**E**) and PCPS (**F**) surface.

Abbreviations: SEM, scanning electron microscope; PC, polyetheretherketone/nano magnesium silicate composite; PCP, PC treated by particle impact; PCPS, PCP treated by concentrated sulfuric acid; SBF, simulated body fluid; EDS, energy dispersive spectrometer.

roughness, hydrophilicity, apatite mineralization, functional groups) of the implantable biomaterials have critical effects on the cells/tissues responses as well as osteogenesis and osseointegration in vivo.[25] In this study, to improve the surface bio-properties of PEEK/n-MS composite (PC), the surface of PC was firstly treated by particle impact (PCP), and subsequently modified by concentrated H_2SO_4 (PCPS). The results revealed that compared to PC with smooth surface, PCP exhibited macroporous surface with pores sizes of about 150 μm (fabricated by particle impact) while PCPS possess not only macropores but also micropores with sizes of about 2 μm (created by sulfonation of PEEK) on the macroporous walls. In addition, many n-MS nanoparticles were exposed on the microporous walls, which created micro-nano structures on PCPS surface. Furthermore, the -SO_3H groups were introduced onto the PCPS surface by the sulfonation (PEEK reaction with concentrated H_2SO_4). Therefore, after treated by particle impact and subsequently modified by concentrated H_2SO_4, PCPS exhibited macro-microporous surface containing micro-nano structures and -SO_3H group.

Compared with PC, the surface roughness of PCP obviously increased due to the production of macropores and some n-MS nanoparticles exposing on the macroporous walls. Moreover, compared with PCP, the surface roughness of PCPS was further enhanced due to the production of micropores on the macroporous walls, and more n-MS nanoparticles exposing on the microporous walls. In addition, compared with PC, the water contact angles of PCP significantly decreased, indicating the increase of hydrophilicity. The improvement of hydrophilicity of PCP was ascribed to the presence of some hydrophilic n-MS exposing on the macroporous surface.[26] Moreover, compared with PCP, the hydrophilicity of PCPS further increased, which was ascribed to the presence of macro-micropores, and more hydrophilic n-MS as well as hydrophilic -SO_3H groups on the microporous surface.

The capability of apatite mineralization of biomaterials in SBF indicates in vitro bioactivity, which is generally considered as a reliable predictor of capacity of osteogenesis and osseointegration in vivo.[27] In this study, the apatite mineralization occurred on all samples (PC, PCP and PCPS), and more apatite particles were formed on both PCP and PCPS than PC. The improvements of apatite formation were attributed to more n-MS exposing on the surfaces of both PCP and PCPS, which induced more apatite formation. The mechanism of apatite formation on these samples was similar to that of the n-MS based composites in SBF,[28] which was shown as

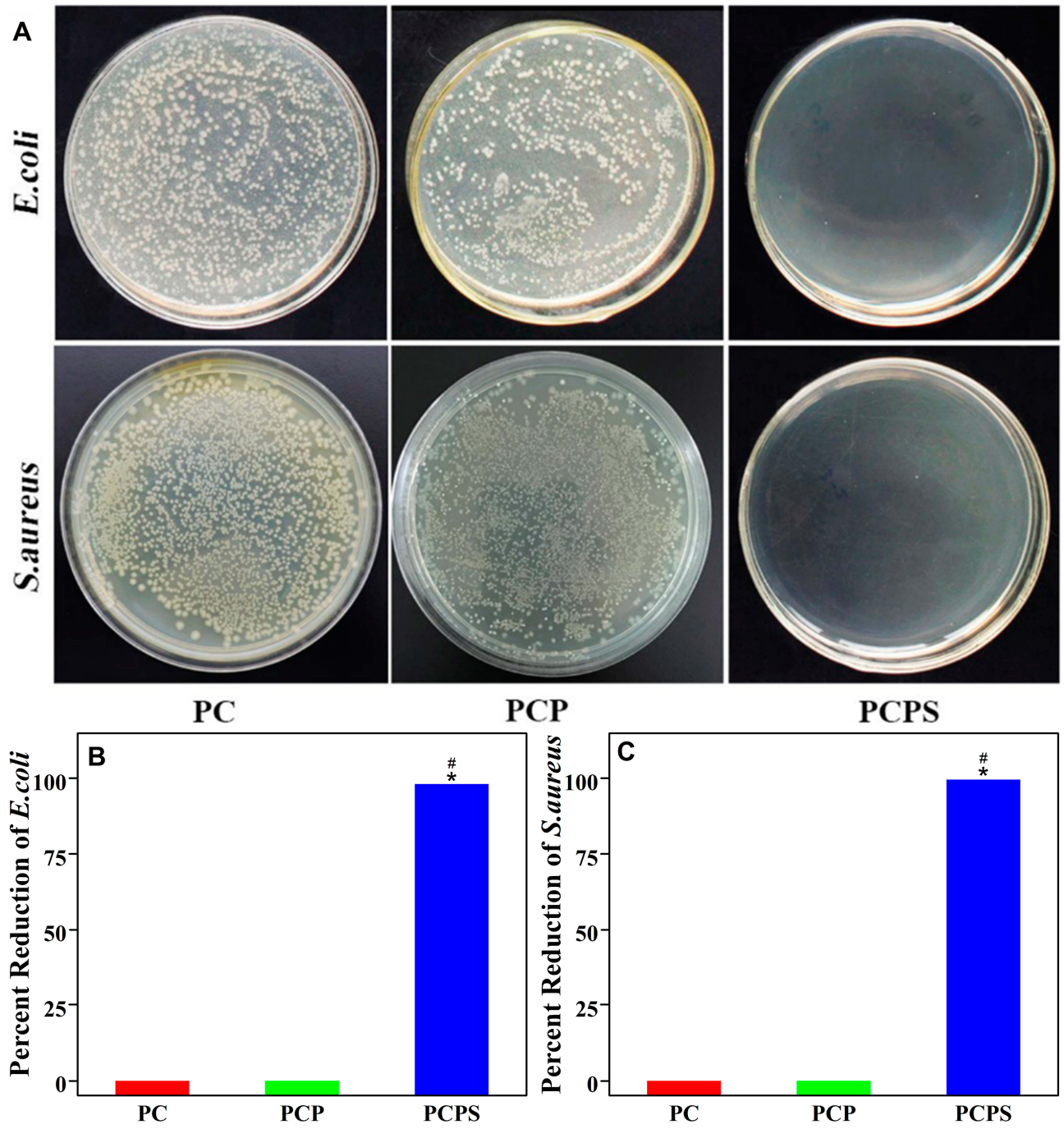

Figure 6 Antibacterial properties of PC, PCP and PCPS: (**A**) *E. coli* and *S. aureus* cultured on the samples (the dilution factor of bacterial suspension seeded on the agar plates for each sample was 100). Percentage reduction: (**B**) *E. coli* and (**C**) *S. aureus* (*represents $p<0.05$, PCPS vs PC; #represents $p<0.05$, PCPS vs PCP).
Abbreviations: PC, polyetheretherketone/nano magnesium silicate composite; PCP, PC treated by particle impact; PCPS, PCP treated by concentrated sulfuric acid; *E. coli*, *Escherichia coli*; *S. aureus*, *Staphyloccocus aureus*.

following: After immersed into SBF, the Ca ions released from the samples due to the slight dissolution of n-MS, which exchanged with H_3O^+ in solution, and then Si-OH formed. After that, the Ca^{2+} was attracted onto the sample surface by electrostatic action, and then PO_4^{3-} was electrostatically attracted by Ca^{2+}, thereby inducing apatite formation.

Bacterial infection is one of the most serious problems for clinical application of the implantable biomaterials, which is the primary cause of implantation failure.[29] Implantable biomaterials with antibacterial performances can inhibit bacterial infection, and thus maintain long-term stability of the implants.[30] Previous studies have shown

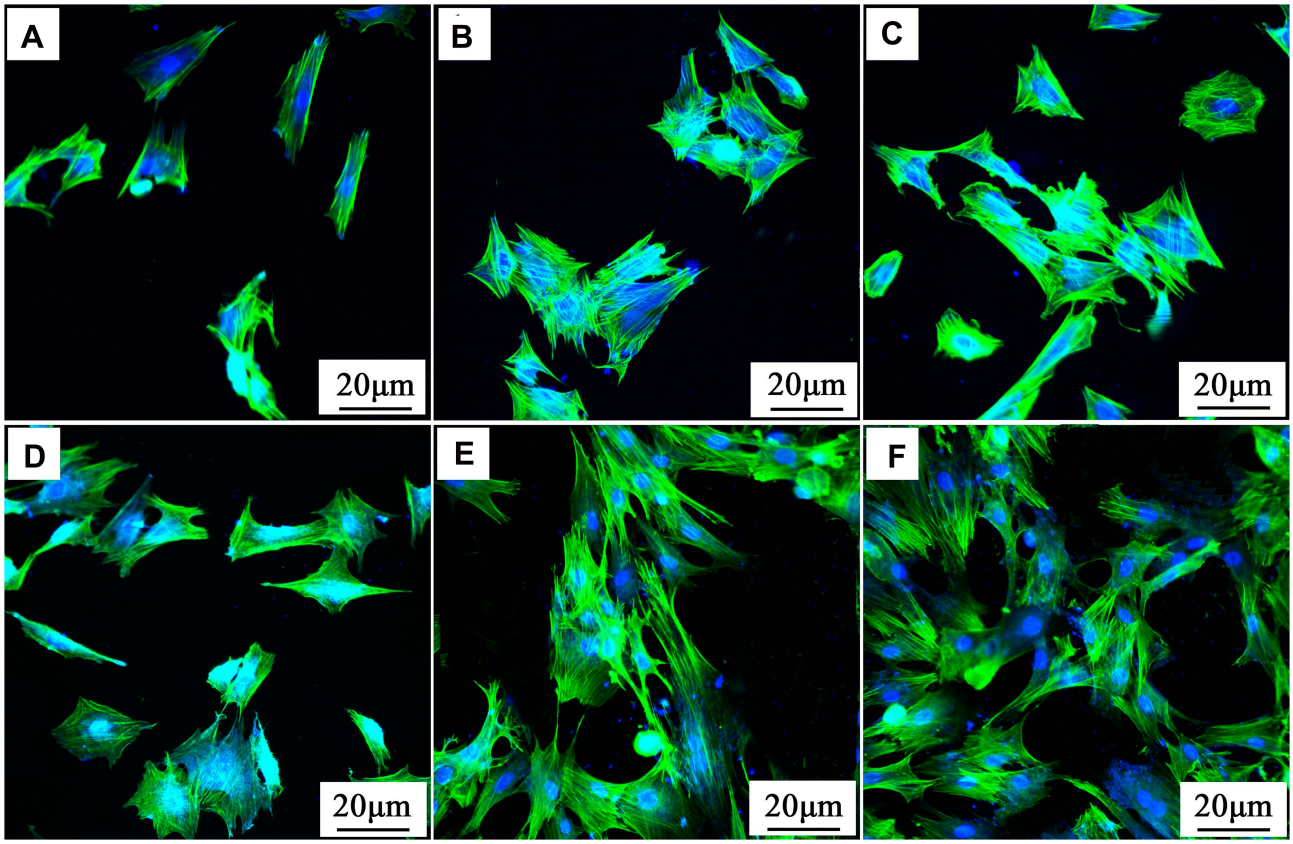

Figure 7 CLSM photographs of morphology of BMSC on PC (**A, D**), PCP (**B, E**) and PCPS (**C, F**) for 12 (**A**–**C**) and 24 hours (**D**–**F**).
Abbreviations: CLSM, confocal laser scanning microscopy; BMSC, bone marrow mesenchymal stem cells; PC, polyetheretherketone/nano magnesium silicate composite; PCP, PC treated by particle impact; PCPS, PCP treated by concentrated sulfuric acid.

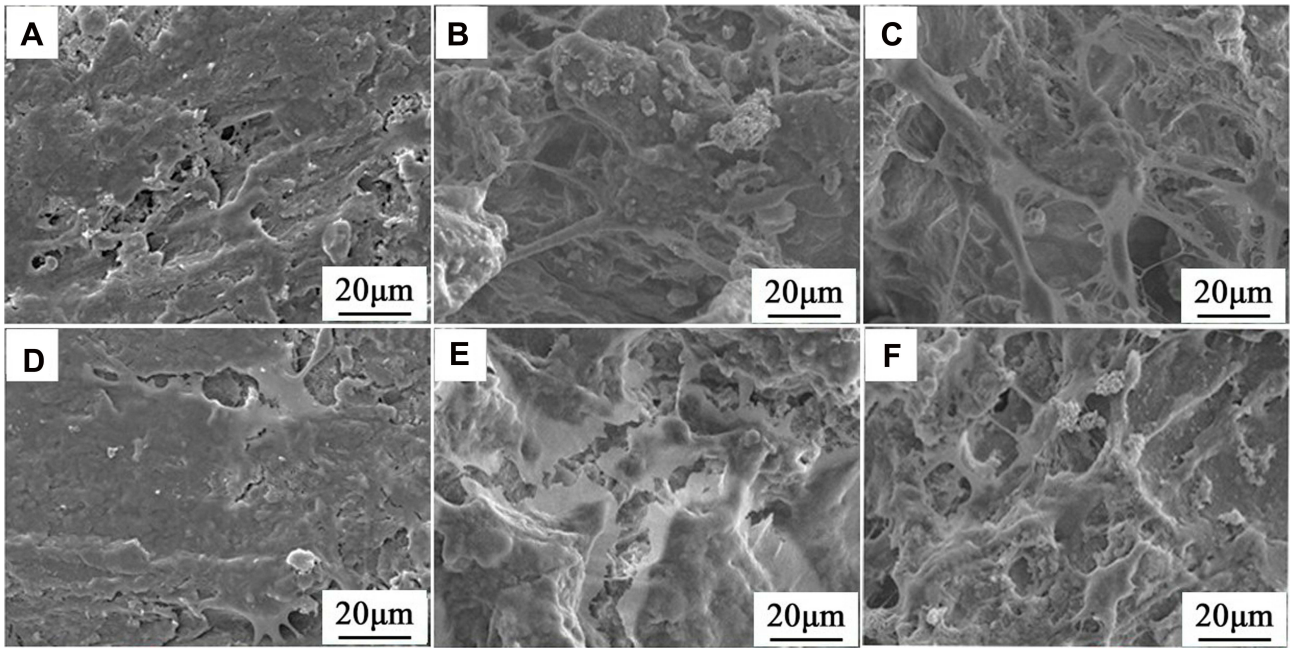

Figure 8 SEM photographs of morphology of BMSC on PC (**A, D**), PCP (**B, E**) and PCPS (**C, F**) after cultured for 3 (**A**–**C**) and 7 days (**D**–**F**).
Abbreviations: SEM, scanning electron microscope; BMSC, bone marrow mesenchymal stem cells; PC, polyetheretherketone/nano magnesium silicate composite; PCP, PC treated by particle impact; PCPS, PCP treated by concentrated sulfuric acid.

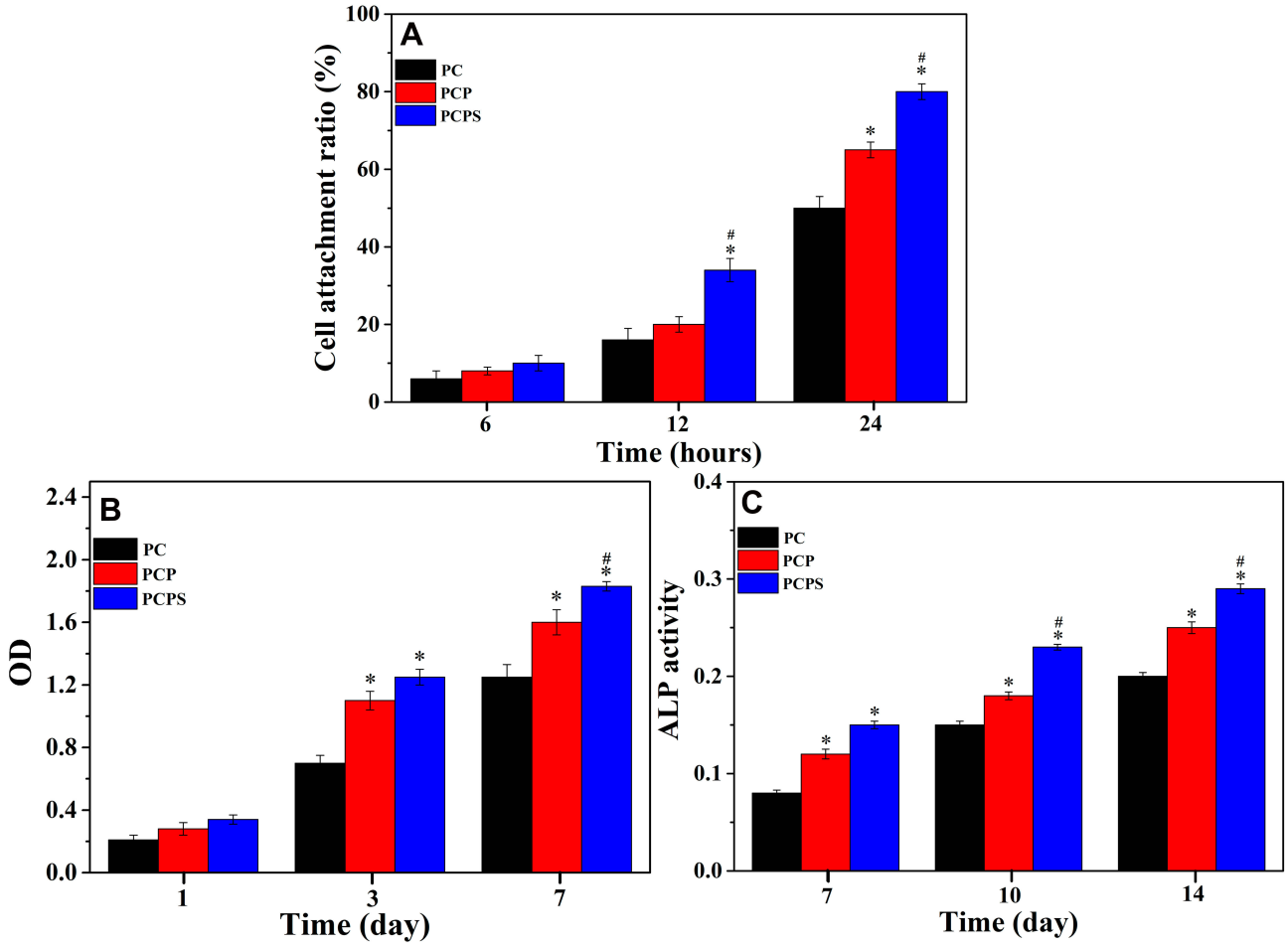

Figure 9 Attachment ratio (**A**), optical density (**B**) and ALP activity (**C**) of BMSC on PC, PCP and PCPS for different days (*represents $p<0.05$, PCPS vs PC, PCP vs PC; #represents $p<0.05$, PCPS vs PCP).

Abbreviations: OD, optical density; ALP, alkaline phosphatase; BMSC, bone marrow mesenchymal stem cells; PC, polyetheretherketone/nano magnesium silicate composite; PCP, PC treated by particle impact; PCPS, PCP treated by concentrated sulfuric acid.

that -SO_3H groups on biomaterials could reduce bacterial adhesion and prevent bacteria from biofilm formation, showing antibacterial performances.[31] In addition, sulfonation of PEEK caused a negatively charged surface, which produced a repulsive force between the negatively charged membranes of bacteria, thereby hindering bacteria attachment.[32] In this study, PC and PCP exhibited no antibacterial activity while PCPS showed antibacterial activity for *E. coli* and *S. aureus* in vitro. Therefore, the antibacterial activity of PCPS was attributed to the presence of -SO_3H groups, which could inhibit the adhesion and growth of bacteria on PCPS.

The adhesion of cells on the biomaterials is initial step of cell-materials interaction, which has significant effects on the subsequent proliferation and differentiation of cells.[33] Furthermore, the surface micro-nano structures of biomaterials provided cells with more binding sites, which might interact with the cellular filopodia at micro-, nano-scales.[34] In this study, the adhesion and spreading of BMSC on PCPS were obviously better than PCP and PC. Therefore, PCPS with micro-nano structural surface significantly promoted cells adhesion and spreading. The adhesion and spreading of the cells on the biomaterial surface are indicators of cytocompatibility, which influences subsequently cells proliferation as well as differentiation.[35] ALP is usually considered as a marker for osteogenic differentiation of the cells.[36] More cells proliferation and differentiation on the biomaterial surface might produce a larger mass of new bone tissues in vivo, which is good for bone repair.[37] In this study, the optical density and ALP activity of cells on PCPS were obviously higher than PCP and PC. Therefore, the results demonstrated that PCPS could significantly enhance the proliferation and osteogenic differentiation of the BMSC.

The surface characteristics (including morphology, nano-micro structure, roughness, hydrophilicity, apatite formation and functional group, etc.) of biomaterials played key roles in facilitating osteoblasts responses (eg, adhesion and spreading as well as proliferation and differentiation, etc.).[38] In this study, as compared with PC and PCP, PCPS exhibited higher roughness and hydrophilicity because of the presence of macro-microporous surface containing micro-nano structures, which caused more n-MS nanoparticles exposing on the surface. Therefore, PCPS with higher surface roughness and hydrophilicity, and macro-microporous surface containing micro-nano structures improved the adhesion and spreading as well as proliferation of the BMSC. Furthermore, as compared with PC, the ability of apatite mineralization of PCPS was obviously enhanced. The mineralized apatite on the biomaterial surface could adsorb serum proteins as well as growth factors, which then promote cells proliferation and differentiation that is closely related to the regeneration of new bone tissues in vivo.[39] Therefore, PCPS with improved apatite mineralization might stimulate the proliferation and differentiation of the BMSC. In summary, our results demonstrated that PCPS with macro-microporous surface containing micro-nano structures obviously enhanced the surface bio-properties, which exhibited antibacterial performances and significantly promoted the cells responses. The positive responses of the BMSC to PCPS were ascribed to the improvement of surface roughness, hydrophilicity and apatite mineralization as well as the presence of macro-microporous surface containing nano-micro structures and functional groups of $-SO_3H$ on the surface, which might be the synergistic effects on cells behaviors. Therefore, PCPS with antibacterial activity and promoting cells responses might have a great potential as bone implant for bone repair.

Conclusion

The surface of PEEK/n-MS composite was firstly treated by particle impact, and subsequently modified by concentrated H_2SO_4. The results showed that PCPS displayed not only macropores but also micropores, and many n-MS nanoparticles appeared on the microporous walls, which constructed micro-nano structural surface. In addition, the surface roughness as well as hydrophilicity of PCPS was significantly improved as compared with PC and PCP. Moreover, the capability of apatite mineralization of PCPS in SBF was remarkably enhanced as compared with PC. Furthermore, PCPS exhibited antibacterial activity for *E. coli* and *S. aureus* due to the introduction of functional groups of $-SO_3H$ on the surface. PCPS significantly promoted the adhesion and spreading, proliferation as well as differentiation of BMSC. In summary, PCPS with macro-microporous surface including $-SO_3H$ groups and micro-nano structures displayed antibacterial properties and promoted cells responses.

Acknowledgments

The study was supported by the National Natural Science Foundation of China (81772343 and 81771990), the youth medical talents funding subject from the 13th five-year plan on science and education strengthening health project of Jiangsu province (QNRC2016356), the key research and development (social development) funding project of Yangzhou city (YZ2018086) and the special funding subject from "the 13th five-year plan on science and education strengthening health project" of Yangzhou city (ZDRC201879).

Disclosure

The authors report no conflicts of interest in this work.

References

1. Yang Y, Yang SB, Wang YG, et al. Anti-infective efficacy, cytocompatibility and biocompatibility of a 3D-printed osteoconductive composite scaffold functionalized with quaternized chitosan. *Acta Biomater*. 2016;46:112–128. doi:10.1016/j.actbio.2016.09.035
2. Li H, Wu CT, Chang J, Ge YS, Chen SY. Functional polyethylene terephthalate with nanometer-sized bioactive glass coatings stimulating in vitro and in vivo osseointegration for anterior cruciate ligament reconstruction. *Adv Mater Interfaces*. 2014;1(5). doi:10.1002/admi.201400027
3. Qiao SC, Cao HL, Zhao X, et al. Ag-plasma modification enhances bone apposition around titanium dental implants: an animal study in Labrador dogs. *Int J Nanomed*. 2015;10:653–664.
4. Liu XW, Chen C, Zhang HZ, et al. Biocompatibility evaluation of antibacterial Ti-Ag alloys with nanotubular coatings. *Int J Nanomed*. 2019;14:457–468. doi:10.2147/IJN.S193569
5. Deng LJ, Deng Y, Xie KN. AgNPs-decorated 3D printed PEEK implant for infection control and bone repair. *Colloid Surface B*. 2017;160:483–492. doi:10.1016/j.colsurfb.2017.09.061
6. Feng P, Peng SP, Wu P, et al. A nano-sandwich construct built with graphene nanosheets and carbon nanotubes enhances mechanical properties of hydroxyapatite-polyetheretherketone scaffolds. *Int J Nanomed*. 2016;11:3487–3500. doi:10.2147/IJN.S110920
7. Zheng YY, Xiong CD, Wang ZC, Li XY, Zhang LF. A combination of CO_2 laser and plasma surface modification of poly(etheretherketone) to enhance osteoblast response. *Appl Surf Sci*. 2015;344:79–88. doi:10.1016/j.apsusc.2015.03.113
8. Zheng YY, Xiong CD, Zhang SL, Li XY, Zhang LF. Bone-like apatite coating on functionalized poly(etheretherketone) surface via tailored silanization layers technique. *Mat Sci Eng C-Mater*. 2015;55:512–523. doi:10.1016/j.msec.2015.05.070
9. Wu JP, Li LL, Fu C, et al. Micro-porous polyetheretherketone implants decorated with BMP-2 via phosphorylated gelatin coating for enhancing cell adhesion and osteogenic differentiation. *Colloid Surface B*. 2018;169:233–241. doi:10.1016/j.colsurfb.2018.05.027

10. Ren YF, Sikder P, Lin BR, Bhaduri SB. Microwave assisted coating of bioactive amorphous magnesium phosphate (AMP) on polyetheretherketone (PEEK). *Mat Sci Eng C-Mater*. 2018;85:107–113. doi:10.1016/j.msec.2017.12.025
11. Mahjoubi H, Buck E, Manimunda P, et al. Surface phosphonation enhances hydroxyapatite coating adhesion on polyetheretherketone and its osseointegration potential. *Acta Biomater*. 2017;47:149–158. doi:10.1016/j.actbio.2016.10.004
12. Shimizu T, Fujibayashi S, Yamaguchi S, et al. Bioactivity of sol-gel-derived TiO_2 coating on polyetheretherketone: in vitro and in vivo studies. *Acta Biomater*. 2016;35:305–317. doi:10.1016/j.actbio.2016.02.007
13. Kargozar S, Kermani F, Beidokhti SM, et al. Functionalization and surface modifications of bioactive glasses (BGs): tailoring of the biological response working on the outermost surface layer. *Materials*. 2019;12(22):3696. doi:10.3390/ma12223696
14. Pang HL, Tian HL, Qiu SB, Wang N, Wang YQ. Progress of titanium strut for cervical reconstruction with nano-graphene oxide loaded hydroxyapatite/polyamide composite and interbody fusion after corpectomy with anterior plate fixation. *Artif Cell Nanomed B*. 2019;47(1):3094–3100. doi:10.1080/21691401.2019.1637883
15. Hajiali F, Tajbakhsh S, Shojaei A. Fabrication and properties of polycaprolactone composites containing calcium phosphate-based ceramics and bioactive glasses in bone tissue engineering: a review. *Polym Rev*. 2018;58(1):164–207. doi:10.1080/15583724.2017.1332640
16. Chan KW, Liao CZ, Wong HM, Yeung KWK, Tjong SC. Preparation of polyetheretherketone composites with nanohydroxyapatite rods and carbon nanofibers having high strength, good biocompatibility and excellent thermal stability. *RSC Adv*. 2016;6(23):19417–19429. doi:10.1039/C5RA22134J
17. Xu AX, Liu XC, Gao X, Deng F, Deng Y, Wei SC. Enhancement of osteogenesis on micro/nano-topographical carbon fiber-reinforced polyetheretherketone- nanohydroxyapatite biocomposite. *Mat Sci Eng C-Mater*. 2015;48:592–598. doi:10.1016/j.msec.2014.12.061
18. Wu ZY, Tang TT, Guo H, et al. In vitro degradability, bioactivity and cell responses to mesoporous magnesium silicate for the induction of bone regeneration. *Colloid Surface B*. 2014;120:38–46. doi:10.1016/j.colsurfb.2014.04.010
19. Cai L, Pan YK, Tang SC, et al. Macro-mesoporous composites containing PEEK and mesoporous diopside as bone implants: characterization, in vitro mineralization, cytocompatibility, and vascularization potential and osteogenesis in vivo. *J Mater Chem B*. 2017;5(42):8337–8352. doi:10.1039/C7TB02344H
20. Kokubo T, Takadama H. How useful is SBF in predicting in vivo bone bioactivity? *Biomaterials*. 2006;27(15):2907–2915. doi:10.1016/j.biomaterials.2006.01.017
21. Diez-Pascual AM, Diez-Vicente AL. Nano-TiO_2 reinforced PEEK/PEI blends as biomaterials for load-bearing implant applications. *ACS Appl Mater Inter*. 2015;7(9):5561–5573. doi:10.1021/acsami.5b00210
22. Brew DRM, Glasser FP. Synthesis and characterisation of magnesium silicate hydrate gels. *Cement Concrete Res*. 2005;35(1):85–98. doi:10.1016/j.cemconres.2004.06.022
23. Montero JFD, Tajiri HA, Barra GMO, et al. Biofilm behavior on sulfonated poly(ether-ether-ketone) (sPEEK). *Mat Sci Eng C-Mater*. 2017;70:456–460. doi:10.1016/j.msec.2016.09.017
24. Russo PA, Antunes MM, Neves P, et al. Solid acids with SO3H groups and tunable surface properties: versatile catalysts for biomass conversion. *J Mater Chem A*. 2014;2(30):11813–11824. doi:10.1039/C4TA02320J
25. Lai PL, Hong DW, Lin CTY, Chen LH, Chen WJ, Chu IM. Effect of mixing ceramics with a thermosensitive biodegradable hydrogel as composite graft. *Compos Part B*. 2012;43(8):3088–3095. doi:10.1016/j.compositesb.2012.04.057
26. Jablonski H, Wedemeyer C, Rekasi H, et al. Laser-induced nanostructures on titanium surfaces as developed in the aeronautics and space industry foster osteoblast activity and function in vitro. *Adv Mater Interfaces*. 2018;5(22). doi:10.1002/admi.201801125.
27. Wu CT, Zhou YH, Lin CC, Chang J, Xiao Y. Strontium-containing mesoporous bioactive glass scaffolds with improved osteogenic/cementogenic differentiation of periodontal ligament cells for periodontal tissue engineering. *Acta Biomater*. 2012;8(10):3805–3815. doi:10.1016/j.actbio.2012.06.023
28. Chen YW, Yeh CH, Shie MY. Stimulatory effects of the fast setting and suitable degrading Ca–Si–Mg cement on both cementogenesis and angiogenesis differentiation of human periodontal ligament cells. *J Mater Chem B*. 2015;3(35):7099–7108. doi:10.1039/C5TB00713E
29. Shen XK, Al-Baadani MA, He HL, et al. Antibacterial and osteogenesis performances of LL37-loaded titania nanopores in vitro and in vivo. *Int J Nanomed*. 2019;14:3043–3054. doi:10.2147/IJN.S198583
30. Escobar A, Muzzio NE, Andreozzi P, et al. Antibacterial layer-by-layer films of poly(acrylic acid)-gentamicin complexes with a combined burst and sustainable release of gentamicin. *Adv Mater Interfaces*. 2019;6(22):1901373. doi:10.1002/admi.201901373
31. Ouyang LP, Zhao YC, Jin GD, et al. Influence of sulfur content on bone formation and antibacterial ability of sulfonated PEEK. *Biomaterials*. 2016;83:115–126. doi:10.1016/j.biomaterials.2016.01.017
32. Tomoglu S, Caner G, Arabaci A, Mutlu I. Production and sulfonation of bioactive polyetheretherketone foam for bone substitute applications. *Int J Polym Mater*. 2019;68(18):1167–1176. doi:10.1080/00914037.2018.1539985
33. Chen SC, Guo YL, Liu RH, et al. Tuning surface properties of bone biomaterials to manipulate osteoblastic cell adhesion and the signaling pathways for the enhancement of early osseointegration. *Colloid Surface B*. 2018;164:58–69. doi:10.1016/j.colsurfb.2018.01.022
34. Xiao QR, Zhang N, Wang X, et al. Oriented surface nanotopography promotes the osteogenesis of mesenchymal stem cells. *Adv Mater Interfaces*. 2017;4(3). doi:10.1002/admi.201600652.
35. Liang LC, Krieg P, Rupp F, et al. Osteoblast response to different UVA-activated anatase implant coatings. *Adv Mater Interfaces*. 2019;6(4). doi:10.1002/admi.201801720.
36. Wang L, Zhang K, Hao YQ, Liu M, Wu W. Osteoblast/bone-tissue responses to porous surface of polyetheretherketone-nanoporous lithium-doped magnesium silicate blends' integration with polyetheretherketone. *Int J Nanomed*. 2019;14:4975–4989. doi:10.2147/IJN.S197179
37. Pina S, Oliveira JM, Reis RL. Natural-based nanocomposites for bone tissue engineering and regenerative medicine: a review. *Adv Mater*. 2015;27(7):1143–1169. doi:10.1002/adma.201403354
38. Zhao Y, Wong HM, Lui SC, et al. Plasma surface functionalized polyetheretherketone for enhanced osseo-integration at bone-implant interface. *ACS Appl Mater Inter*. 2016;8(6):3901–3911. doi:10.1021/acsami.5b10881
39. Zhao SC, Zhang JH, Zhu M, et al. Three-dimensional printed strontium-containing mesoporous bioactive glass scaffolds for repairing rat critical-sized calvarial defects. *Acta Biomater*. 2015;12:270–280. doi:10.1016/j.actbio.2014.10.015